The Geological Society of America
Special Paper 550

Mars Crater Database: A participative project for the classification of the morphological characteristics of large Martian craters

A. Lagain[1,2,*†], S. Bouley[1,3†], D. Baratoux[4†], C. Marmo[1†], F. Costard[1†], O. Delaa[1†], A. Pio Rossi[5†], M. Minin[5†], G.K. Benedix[2†], M. Ciocco[1], B. Bedos[1], A. Guimpier[1], E. Dehouck[6,7], D. Loizeau[7], A. Bouquety[1], J. Zhao[1,8], A. Vialatte[9], M. Cormau[1], E. Le Conte des Floris[1], F. Schmidt[1], P. Thollot[7], J. Champion[10,11], M. Martinot[7,12], J. Gargani[1], P. Beck[9,13], J. Boisson[14], N. Paulien[1], A. Séjourné[1], K. Pasquon[1], N. Christoff[15,16], I. Belgacem[1], F. Landais[1], B. Rousseau[17], L. Dupeyrat[1], M. Franco[18,19], F. Andrieu[17], B. Cecconi[17], S. Erard[17], B. Jabaud[1], V. Malarewicz[1], G. Beggiato[1], G. Janez[1], L. Elbaz[1], C. Ourliac[1], M. Catheline[1], M. Fries[1], A. Karamoko[1], J. Rodier[1], R. Sarian[1], A. Gillet[1], S. Girard[1], M. Pottier[1], S. Strauss[1], C. Chanon[1], P. Lavaud[1], A. Boutaric[1], M. Savourat[1], E. Garret[1], E. Leroy[1], M.-C. Geffray[1], L. Parquet[1], M.-A. Delagoutte,[1] and O. Gamblin[1]

[1]*Geosciences Paris-Sud (GEOPS), Paris-Saclay University, Centre National de la Recherche Scientifique (CNRS), 91405 Orsay, France*
[2]*Space Science and Technology Centre, School of Earth and Planetary Sciences, Curtin University, Perth, Western Australia 6845, Australia*
[3]*Institut de Mécanique Céleste et de Calcul des Ephémérides, UMR8028, 77 avenue Denfert-Rochereau, 75014 Paris, France*
[4]*Géosciences Environnement Toulouse, UMR 5563 CNRS, Institut de Recherche pour le Développement (IRD), University of Toulouse, 14 Avenue Edouard Belin, 31400 Toulouse, France*
[5]*Jacobs University Bremen, Physics and Earth Sciences, 28759 Bremen, Germany*
[6]*Institut de Recherche en Astrophysique et Planétologie (IRAP), CNRS, Université Paul Sabatier–Toulouse III (UPS), Centre National d'Études Spatiales (CNES), 31400 Toulouse, France*
[7]*Laboratoire de Géologie de Lyon–Terre, Planètes, Environnement (LGL-TPE), University of Lyon, Université Claude-Bernard Lyon 1 (UCBL), and École Normale Supérieure de Lyon (ENSL), CNRS, 69622 Villeurbanne, France*
[8]*Department of Earth System Science, Tsinghua University, Beijing 100084, China*
[9]*Institut de Planétologie et d'Astrophysique de Grenoble, University Grenoble Alpes, 38058 Grenoble, France*
[10]*Observatoire Midi-Pyrénées (OMP), IRAP, UPS, 31400 Toulouse, France*
[11]*CNRS, IRAP, 9 Avenue du Colonel Roche, BP 44346, 31028 Toulouse Cedex 4, France*
[12]*Faculty of Science, Vrije University Amsterdam, De Boelelaan 1085, 1081 HV Amsterdam, Netherlands*
[13]*Institut Universitaire de France, 75005 Paris, France*
[14]*Société Nationale des Chemins de fer Français (SNCF) Reseau, Engineering & Projects Headquarter, Railroad and Environment Department, Natural Hazards Division, 75014 Paris, France*
[15]*Faculty of Telecommunications, Technical University of Sofia, Boulevard Kliment Ohridski 8, 1796 Sofia, Bulgaria*
[16]*Laboratoire d'Astrophysique de Marseille (LAM), Université d'Aix-Marseille (UAM), CNRS, CNES, 13388 Marseille, France*
[17]*Laboratoire d'Études Spatiales et d'Instrumentation en Astrophysique (LESIA), Observatory of Paris, Paris Sciences et Lettres (PSL) University, CNRS, Sorbonne University, University of Paris, 5 place Jules Janssen, 92195 Meudon Cedex, France*
[18]*Laboratoire d'Astrophysique (AIM), University Paris Diderot, Sorbonne Paris Cité, Commissariat à l'Énergie Atomique et aux Énergies Alternatives (CEA), CNRS, F91191 Gif-sur-Yvette, France*
[19]*Centre for Astrophysics Research, Department of Physics, Astronomy & Mathematics, University of Hertfordshire, College Lane, Hatfield AL10 9AB, UK*

*anthony.lagain@curtin.edu.au
†These authors contributed to writing this paper. Other authors were solely involved in building the database.

Lagain, A., Bouley, S., Baratoux, D., Marmo, C., Costard, F., Delaa, O., Pio Rossi, A., Minin, M., Benedix, G.K., Ciocco, M., Bedos, B., Guimpier, A., Dehouck, E., Loizeau, D., Bouquety, A., Zhao, J., Vialatte, A., Cormau, M., Le Conte des Floris, E., Schmidt, F., Thollot, P., Champion, J., Martinot, M., Gargani, J., Beck, P., Boisson, J., Paulien, N., Séjourné, A., Pasquon, K., Christoff, N., Belgacem, I., Landais, F., Rousseau, B., Dupeyrat, L., Franco, M., Andrieu, F., Cecconi, B., Erard, S., Jabaud, B., Malarewicz, V., Beggiato, G., Janez, G., Elbaz, L., Ourliac, C., Catheline, M., Fries, M., Karamoko, A., Rodier, J., Sarian, R., Gillet, A., Girard, S., Pottier, M., Strauss, S., Chanon, C., Lavaud, P., Boutaric, A., Savourat, M., Garret, E., Leroy, E., Geffray, M.-C., Parquet, L., Delagoutte, M.-A., and Gamblin, O., 2021, Mars Crater Database: A participative project for the classification of the morphological characteristics of large Martian craters, *in* Reimold, W.U., and Koeberl, C., eds., Large Meteorite Impacts and Planetary Evolution VI: Geological Society of America Special Paper 550, p. 629–644, https://doi.org/10.1130/2021.2550(29).

ABSTRACT

The most recent comprehensive database of Martian impact craters was the result of the work of impact crater scientists (S.J. Robbins and B.M. Hynek) who carefully examined the available high-resolution imagery of Mars. Building on this previous work, we present the result of an alternative approach involving 56 planetary scientists and trained students. A web platform was designed for this purpose. All impact craters larger than 1 km in diameter were classified according to a simplified classification scheme, recording the primary or secondary nature of the crater, and the morphology of the ejecta (single, double, or multiple layered ejecta rampart sinuous [LERS], or low-aspect-ratio layer ejecta [LARLE]). In total, 8445 LERS craters, 24,530 partially buried craters, 55,309 secondary craters, and 288,155 craters in the category "standard" were identified. Our assessment differs for 8145 entries in the original database compiled by Robbins and Hynek, which are not considered to be impact structures. In this work, ~39,000 secondary craters have been associated with 108 primary craters. Coupled to the existing database, the database we propose here offers a complementary way to investigate the geological history of Mars. More specifically, the completion of layered ejecta crater morphologies down to 1 km and the connection established between secondary and primary impact crater sources will allow the implementation of statistical studies to reveal the spatial and temporal evolution of the impacted material characteristics. Thanks to the simplified classification we performed here, this version of the database can be easily used as a training data set for crater identification algorithms based on machine-learning techniques with the aim to identify smaller impact craters and to automatically define their morphological characteristics. Since it is not possible to confirm an impact structure from remote-sensing data alone, any Martian impact database at this stage remains subjective, and its assessment must be facilitated. The interface we developed for this participative project can be directly used for this purpose and for continuous updates and improvements of this work, in particular, with the latest high-resolution imagery releases such as the CTX global mosaic by J.L. Dickson and others, but also as a platform for building specific databases of craters or any other structures located in a particular region of interest.

INTRODUCTION

The determination of ages of surfaces of rocky and icy bodies of the solar system is one outstanding challenge in planetary science. Applications of radiometric methods, typically used for terrestrial rock samples, to extraterrestrial samples, and the significance of these results for the global picture of planetary evolution are yet limited by several obstacles. Ages from the *Apollo* samples are—and will remain for the next decades—the major contribution to our understanding of the chronology of the Moon, Mars, and the asteroids of the main belt. Ages of the meteorites from Mars, or the Moon, cannot be assigned with certainty to a particular source on the surface. The recent breakthroughs enabling in situ isotopic analyses on rovers (e.g., first K-Ar ages on Mars; Farley et al., 2014) are extremely valuable, but the numbers of ages that can be obtained by these techniques are necessarily constrained by the limited mobility of the rover. The continuous exposure of a planetary surface to meteoritic bombardment offers a major tool to planetary scientists to map planetary surfaces and determine the chronology of various geological processes, including volcanism, tectonic deformation, erosion and transport, and impact cratering itself (Hartmann and Neukum, 2001). In addition, in the case of Mars, the morphology of impact craters themselves, and their distribution in time and space, may be used to constrain the past presence and spatial extent of subsurface volatiles, and in the end, the climatic evolution of the planet (Barlow and Perez, 2003; Barlow, 2004; Jones and Osinski, 2015; Warren et al., 2019).

Such investigations are facilitated by the availability of reliable catalogs of impact craters. Previous workers took advantage of new imagery to refine and update earlier crater databases down to smaller and smaller diameters (Costard, 1989; Barlow and Bradley, 1990; Barlow and Perez, 2003). As the number of impact structures increases exponentially with smaller sizes, the acquisition of data for objects smaller than 5 km in diameter becomes particularly tedious. Several attempts have been made to automatically identify craters using imagery or elevation data, but these techniques produce false detections, and the identification proves to be incomplete (~70%) and depend on the algorithm architecture and other parameters such as type of terrain, crater

morphologies, data set used (digital elevation model [DEM], imagery, etc.), and training data set (Urbach and Stepinski, 2009; Salamunniccar et al., 2012; Lee, 2019). Recent improvement of the technique has nevertheless allowed ~90% true detection to be reached for kilometric craters on Mars (Benedix et al., 2020a), thanks in particular to the quality and the size of the crater catalog used to train the algorithm (~7000 craters among the 385,000 entries of the database compiled by Robbins and Hynek, 2012). However, this technique does not allow a classification of detected impact craters, with multiple entries relevant for future scientific studies, including primary or secondary origin, the morphology of the ejecta blanket, and the degradation state.

The visual identification by impact scientists of impact craters on planetary surfaces is a subjective task (Robbins et al., 2014) but remains the most widely accepted approach. The subjectivity of this technique leads to up to 35% of difference in terms of number of craters reported over the same region between different experts for subkilometric craters on the Moon. The most complete human-made Martian crater database contains 384,399 craters larger than 1 km in diameter (Robbins and Hynek, 2012). For craters $\geq$ 3 km in diameter, corresponding to 21% of the database (~85,000 entries), elevation, morphologic, and morphometric information is available. For a large proportion of smaller impact craters, only size, location, and primary/secondary categorization are provided, i.e., 79% of the catalog. According to the authors, this database would be amenable to computing surface crater retention ages if partially or totally buried and secondary craters were removed. Furthermore, this catalog was never formally assessed by different experts after the peer-review process and publication. This type of assessment could potentially lead to a wider acceptance in the community of Martian scientists (98 citations of Robbins and Hynek [2012, 2014] in January 2020). These gaps represent one of the motivations of this work.

This study therefore had the objective to provide complementary information and added value to the Robbins and Hynek's catalog. For this purpose, a large group was formed, composed of planetary scientists and students carefully trained to conduct impact identification and classification. Each member of the group was tasked with the objectives to check the validity of a segment of the catalog and check for missing craters. In addition, the participants had to classify each impact crater according to its morphology by using the classification scheme discussed in the next section. A second important objective was complete the morphological information for craters smaller than 3 km in diameter. The advantages of gathering a large group are to reduce the tedious workload per individual and allow multiple checks, which increase the final robustness of the observations and classifications. The morphological classification was performed using the Thermal Emission Imaging System (THEMIS) mosaic, which provides complete coverage of the surface of Mars at a resolution of 100 m per pixel (Christensen et al., 2004). Mars Obiter Laser Altimeter (MOLA; Smith et al., 2001) data were also used to distinguish buried impact structures. The common guidelines and platform designed for this investigation are described in the "Procedure for Adding Information to the Database" section, along with the necessary correction procedures following the integration of observations from multiple researchers. The analysis of this catalog is discussed in "Results and Discussion" section. Precautions and directions for possible investigations using the Mars Crater Database and other crater catalogs are discussed in concluding section.

CRATER CLASSIFICATION

Each crater in the database was classified into one of the four classes described below. Here, we bring the reader's attention to the fact that this classification and its subsequent results do not replace the classification made by Robbins and Hynek (2012); instead, we had the aim to provide future users with an alternative point of view regarding the morphological information contained in the database and complete it for diameter (D) $\leq$3 km.

(1) Layered ejecta rampart sinuous (LERS) and low-aspect-ratio layered ejecta (LARLE) craters: Primary impact craters for which the ejecta blankets are continuous and exhibit sinuous termini (Barlow et al., 2000; Costard, 1989) were classified as LERS craters. Low-aspect-ratio layered ejecta (LARLE) craters (Barlow et al., 2014; Boyce et al., 2015) were also classified in this category. Some examples are given on Figure 1A. The LERS craters were also subclassified following the following standard classification (Barlow et al., 2000), including single (SLERS), double (DLERS), and multiple ejecta layers (MLERS). Radial (Rd) and circular ejecta morphologies, such as pancake craters (Barlow et al., 2000), were excluded from this category and were classified in the "standard" crater category (see point 4).

(2) Secondary craters: Despite the fact that Robbins and Hynek (2014) already identified ~70,000 secondary craters in their database, a preliminary analysis revealed that some entries were likely inconsistent with a secondary origin (see Supplemental Material Appendix A[1]). We classified impact craters as secondary craters following the same criteria used by Robbins and Hynek (2014) and inspired by several studies (Shoemaker, 1962, 1965; Oberbeck and Morrison, 1974; McEwen and Bierhaus, 2006; Robbins and Hynek, 2011a, 2011b; Quantin et al., 2016): "[i] Is the crater entrained within a chain, elongate crater group, and/or has a 'herringbone' ejecta pattern? [ii] Is the crater highly elliptical with the long axis radial to a much larger crater? [iii] Does the crater appear to have been 'scooped' out at an angle with the shallower part radially away from a larger crater?" (Robbins and Hynek, 2014, p. 67). If a crater fit one of these criteria, it was marked as a secondary crater. Some examples classified in this category are found in Figure 1B. A regional analysis was essential to identify possible relationships with a primary crater, and this was based on clustering and alignments. If the orientations of asymmetric craters in the surveyed population

[1]Supplemental Material. Completed version of the Mars Crater Database created in this study. Please visit https://doi.org/10.1130/SPE.S.14233577 to access the supplemental material, and contact editing@geosociety.org with any questions.

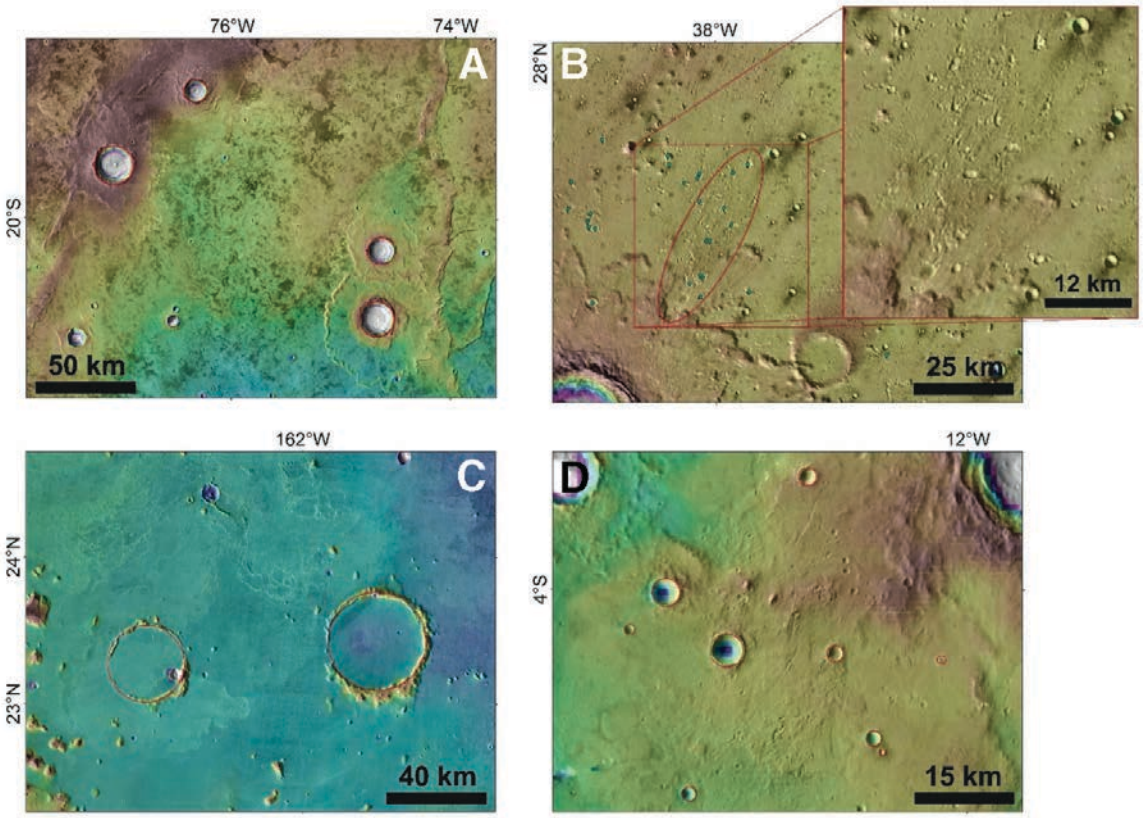

Figure 1. Mars Orbiter Laser Altimeter (MOLA) data superposed onto daytime infrared Thermal Emission Imaging System (THEMIS) mosaic showing some examples of impact craters classified into each of the four categories. Craters are symbolized by red circles that fit their rim. (A) Four layered ejecta rampart sinuous (LERS) craters located in Solis Planum. (B) Clusters of secondary craters formed as a consequence of the formation of the Calahorra primary impact crater in Chryse Planitia, visible at the lower-left corner of the image. (C) Two impact craters located on Amazonis Planitia recognized as "buried/degraded" according to the criteria established in this study. (D) Nine impact craters classified as "standard" in Meridiani Planum.

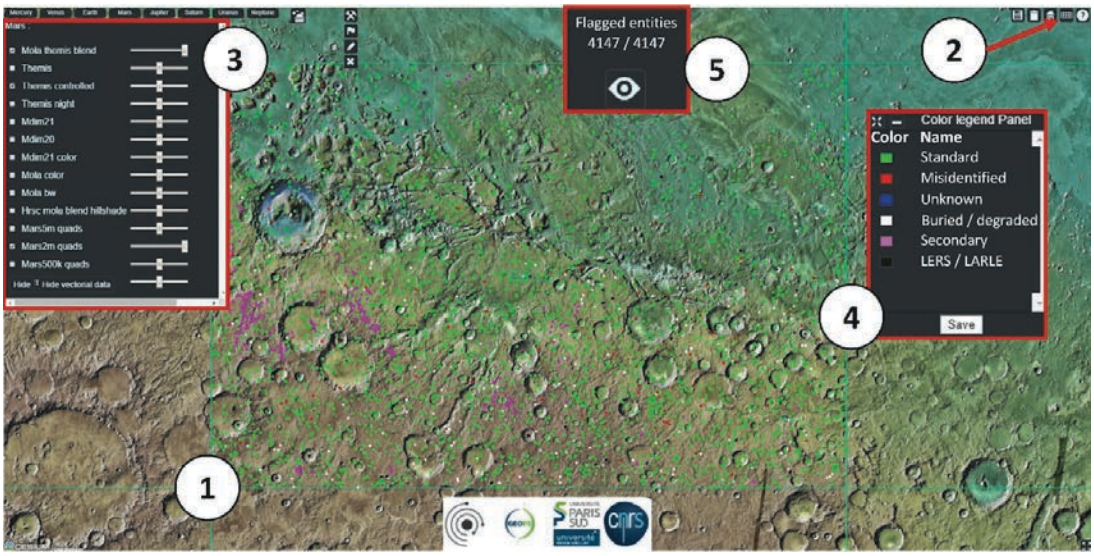

Figure 2. Principal functionalities of the interface: (1) Mars 2M quads corresponding to the division of the database, the limit of quadrangles considered in this study; (2) projection mode (planisphere or globe); (3) data panel allowing display of one or more data set with transparency level; (4) legend panel grouping the four main categories as well as flagging uncertain and misidentified entries; (5) number of displayed impact craters and number of displayed impact craters that are already classified. Each colored dot corresponds to an impact crater in the Robbins and Hynek (2012) database.

had ejecta pointing away from a potential source primary crater, the CRATER-ID of the plausible primary crater is mentioned in the ORIGIN column of each secondary impact crater entry in the database (see Supplemental Material Appendix B). This association was added if the primary impact crater source could be identified according to the criteria developed by Robbins and Hynek (2011a, 2011b), and if the associated secondary population (secondary impact craters having the same origin) exceeded 50 impact craters (arbitrarily fixed).

(3) Buried/degraded craters: Impact craters exhibiting a high degree of degradation, such as those for which the elevation of their floor was approximately equal to that of the surrounding terrain or those with a flat floor mainly filled up by sedimentary or volcanic material (Barata et al., 2012), implying they are actually partially buried, were classified in this category. Such impact craters must indeed be generally excluded from crater counts because their formation occurred before the dated surface (Craddock et al., 1997; Barlow, 1995). Examples of buried/degraded craters are shown on Figure 1C. Some of them can nevertheless be used for specific purposes (such as dating basement units, or old surfaces covered by volcanic or sedimentary material). This point will be developed and discussed later herein.

(4) All other impact craters: Craters that could not be attributed to one of the three previous categories were classified in a fourth category named "standard" in this study (Fig. 1D). This category may include impact craters superposed onto the surrounding ground, background secondary craters, and craters without ejecta, or with a blanket that was not continuous enough or sinuous enough to be classified as LERS or LARLE craters (such as radial ejecta, pancake or pedestal craters; Barlow et al., 2000; Kadish and Head, 2014).

PROCEDURE FOR ADDING INFORMATION TO THE DATABASE

Development of a Platform for the Revision of the Impact Crater Catalog

Visual examination of ~385,000 impact craters is a particularly long task, and it would be difficult to perform by only one person (taking ~133 [at 8 h per day] working days for a single person, assuming 10 s spent on each crater, including the time required to move from one crater to another). A platform allowing collaborative research between planetary scientists was therefore developed at the Geosciences Paris Sud (GEOPS) laboratory. This platform and the distribution of the workload between the different participants made the workload for each participant reasonable and the examination of craters an enjoyable experience. The regional context of some of the craters can potentially provide a clue with which to correctly identify and classify a particular crater. It was therefore essential to not use individual images covering the immediate surroundings of each crater, but instead use a data set allowing the participant to navigate at distance around each crater at different resolutions. The most appropriate controlled imagery mosaic, at the time of writing, covering the entire surface of Mars at a resolution that allowed identification of impact craters larger than 1 km in diameter was the Thermal Emission Imaging System (THEMIS) data mosaic. Therefore, the visual assessment was performed using these images. We hypothesized that some craters may not have been included (missing entries) in the database of Robbins and Hynek (2012). This data set enabled the exploration of the entire surface of Mars in order to identify and to add potential new entries to our database, if necessary. The use of the THEMIS daytime infrared (IR) mosaic nevertheless entailed the visualization of a very small portion of the surface of Mars with a low resolution, since this mosaic was created with both low-quality and high-quality images. This may have led to a misinterpretation of crater morphology, but these misinterpretations should be limited to a low number of cases (a few tens of cases to a few hundred cases) compared to the number of craters contained in the original database (Barlow, 2017).

A Web interface was developed using the open-source JavaScript library Cesium (https://cesiumjs.org/). Cesium is a geographic information system (GIS) library optimized for three-dimensional (3-D) mapping. Cesium was specifically designed for Earth-based applications. We therefore implemented planetary geographic standards for its use. In brief, our interface has some interesting advantages:

(1) an effective and easy-to-use data navigation system,
(2) a web client that does not require complex setup for local installation of dedicated software,
(3) effective simultaneous access by distant users on different operating systems and Web browsers,
(4) a precise georeferenced framework for visualization,
(5) easy integration of global imagery data of Mars, distributed by the U.S. Geological Survey (USGS), such as MOLA or THEMIS data sets, and
(6) the possibility to adapt the interface for assessment of crater catalogs.

This last point is developed in the next section.

Training, Distribution of the Database, and Revision Using the Cesium Platform

The catalog published by Robbins and Hynek (2012) was first divided into 140 quadrangles corresponding to the Mars 2M quad cartographic regions defined by the USGS (Fig. 2). The data divided in this way were stored in 140 geoJSON files. GeoJSON is an open standard format designed for representing simple geographic features and their attributes; it is based on JSON, the JavaScript Object Notation, and hence it is particularly adapted for Web applications (http://geojson.org/). Each of these files was distributed to 56 collaborators (see Supplemental Material Appendices C and D). The selected participants included planetary scientists, astronomers, or geologists that has been previously trained on the recognition of the diversity of impact crater morphologies and the utilization of the Web interface. A tutorial

detailing the usage of the interface and containing many examples of craters in each category was distributed to each participant. We also distributed a testing quadrangle located at the north part of Chryse Planitia, where all craters have been classified, allowing each user to visualize the complete diversity of crater morphologies investigated in the classification.

Figure 2 gives an overview of the appearance of the interface on the screen of each user. Label 1 on Figure 2 corresponds to the geographic limits of one GeoJSON file corresponding to a Mars 2M quadrangle. The interface provides 3-D and 2-D (simple cylindrical projection) visualization modes (see label 2 on Fig. 2). Each file may be examined and revised independently of the others, and the entire THEMIS imagery set remains accessible when a given GeoJSON file is uploaded on the interface in order to avoid edge effects. Once a part of the catalog is loaded in the interface, the user has the possibility to visualize the surface through different data sets and set up the transparency level of each one (see label 3 on Fig. 2). For the purpose of this study, all participants chose the THEMIS DAY IR mosaic overlaid to the MOLA data set, at 50% of transparency level, throughout the entire revision. The catalog was loaded into the interface by a simple drag and drop of the GeoJSON files from the local computer disk. Each entry of a GeoJSON file corresponds to a crater with its location, its size, and its identification number, information given by Robbins and Hynek (2012). When new craters (not present in the original database) are identified from THEMIS imagery or MOLA data set, the user has the option to add a crater and define its size and position based on two or three points placed manually on the rim using an in-house developed widget. The crater diameter is determined from the circle that is automatically fitted to these points.

Crater classification was performed via a specific flag widget (a simple click on one of the entries of the list of crater classes, corresponding to label 4 on Fig. 2). The class "uncertain" allows users to report that they are unable to apply to a certain crater one of the classes proposed in this study. Furthermore, the class "misidentified entry" gives the users the possibility of flagging an unrecognizable impact structure for the place and diameter described in the database of Robbins and Hynek. The crater then appears with a specific color-code (a different color is assigned to each crater class). The legend panel (label 4 on Fig. 2) can be also saved (with the specific extension "legendjson") for future use. If such a file is already available, it can be loaded by a simple drag and drop in the legend panel. The result of the classification can be saved on the local computer and reloaded later, allowing the processing of a GeoJSON file in several sessions. A flag counter displays the number of entities already classified (see label 5 on Fig. 2); this is useful to resume ongoing revision of a part of the catalog by the same user, or for the examination and double-checking of the work of a given participant. With our interface, it is possible to classify impact craters at a rate of 200–500 craters per hour (7–18 s for each crater), depending on crater density and morphological complexity of each crater. Examination of the entire catalog of Martian craters would thus represent a total workload of ~800–2000 h, which corresponds to a reasonable average workload of ~14–36 h per participant.

An additional global check was performed by A. Lagain once the work was achieved. This process had the objective to (1) correct the possible mistakes of less experienced participants and provide feedback to improve the processing of the next file assigned, and (2) assign "uncertain" craters into one of the other classes, where appropriate. If needed, this step made use of the higher-resolution CTX data (6 m/pixel), when available. At this step, each layered ejecta crater was also classified into one of the four subclasses of this class: SLE, DLE, MLE, and LARLE craters. Details about the revision team and the contribution of each participant are given in the Supplemental Material Appendices C and D.

RESULTS AND DISCUSSION

The catalog obtained following the assessment of the database compiled by Robbins and Hynek (2012) by the group using the Cesium platform contains 384,582 entries, of which 74.9% (288,155) are classified as "standard," 2.2% (8445) are LERS craters, 6.4% (24,530) are buried/degraded craters, and 14.4% (55,309) are secondary craters. Finally, 8145 misidentified entries (2.1%) were identified from Robbins and Hynek's database. Figures 3 and 4 present, respectively, the incremental

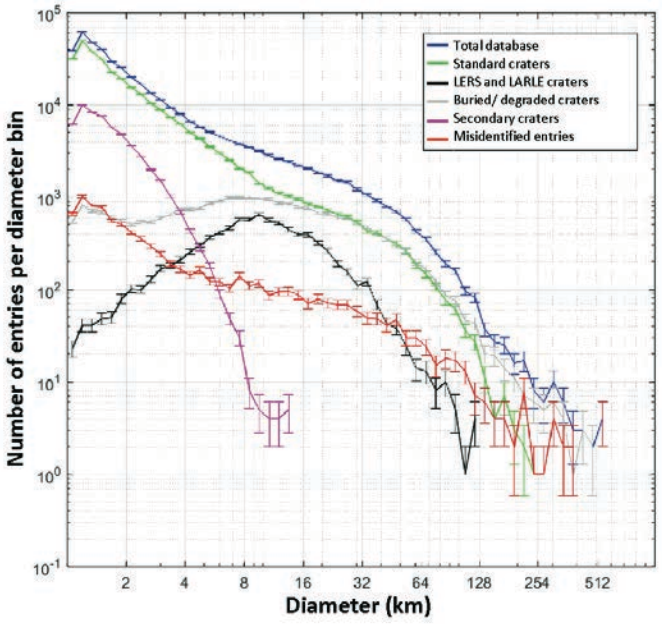

Figure 3. Incremental crater size-frequency distribution of the four types of craters classified in this study as well as misidentified entries. Craters are binned in $2^{1/6}D$ rather than the classical $2^{1/2}D$ intervals due to the large number of craters and the large panel of diameters analyzed in this study. Error bars were calculated by the square-root of the counts in the incremental size-frequency bin divided by the counts in the bin for each crater class (Crater Analysis Techniques Working Group, 1979). LERS—layered ejecta rampart sinuous; LARLE—low-aspect-ratio layer ejecta.

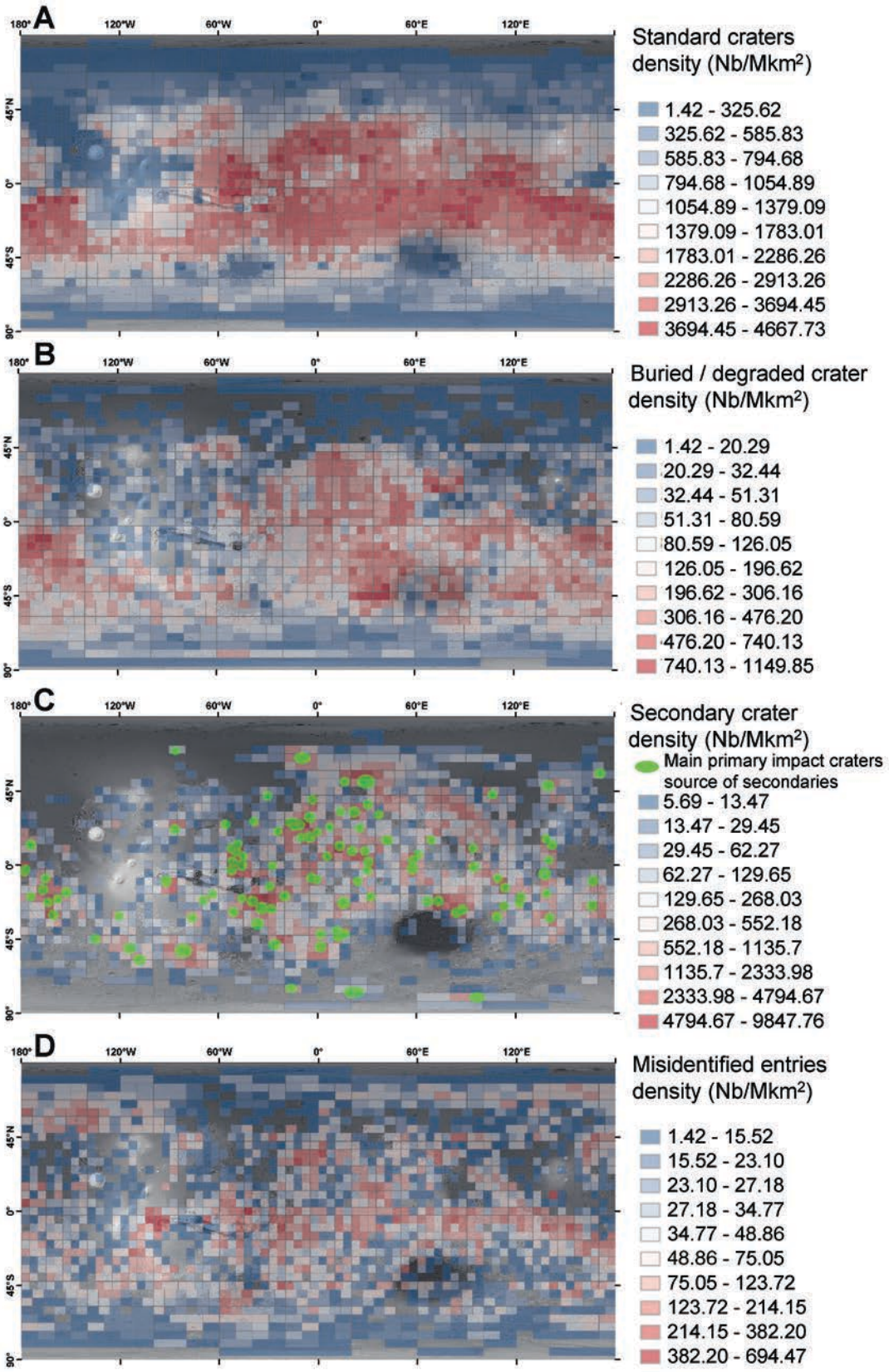

Figure 4. Crater density maps according to the category assigned in this study. The grid used to build these density maps was the U.S. Geological Survey grid at 1:500,000 scale. (A) Density of standard impact craters. A high cratering density for this type of impact craters is observed on highlands, south of the dichotomy. Northern lowlands, the Tharsis region, and terrains at latitudes higher than 45°N and 45°S exhibit low density due to the intensity of resurfacing processes (affecting small craters). (B) Density of buried or degraded craters. This category of craters is mainly represented on southern highlands terrains because of the age of these regions. (C) Secondary impact crater density and 108 primary craters that have produced 70% of the identified secondary crater population for *D* (diameter) >1 km. Red spots in northern Isidis Planitia where no primary impact craters have been recognized as source of secondaries is due to distant secondary craters from Lyot crater. (D) Misidentified entries density in the catalog of Robbins and Hynek (2012). The entries recognized as misidentified in our survey are mainly distributed around the dichotomy and tectonic and volcanic regions, where pseudocircular geological structures are highly concentrated.

crater size-frequency distribution of the four categories as well as misidentified entries and their geographic distribution, which are described in detail in the following sections, while Figures 5 and 6 detail and compare the size-frequency and geographic distributions of LERS and LARLE impact craters with other databases compiled in previous studies.

Standard Impact Craters and Added Entries

The distribution of "standard impact craters" is closely related to the surface age (Fig. 4A). A high cratering density of this type is observed on highlands areas, whereas a low density is observed on northern lowlands and on the Tharsis bulge. From 45° latitudes, a decreasing cratering density is observed with increasing latitude. This observation is interpreted to be the result of the presence of polar caps and enhanced efficiency of resurfacing processes.

Among 185 added entries, half of them are less than 2 km in diameter. It is possible that these small craters were identified by Robbins and Hynek (2012), but that their diameter was underestimated (<1 km in diameter), and the crater was removed from the published database. The low number of new entries identified in our survey is not astonishing since the influence of erosion processes, and more generally all surface processes, on large crater morphologies is limited compared to subkilometric craters, leading thus to a lower degree of subjectivity in the identification of kilometric craters than those smaller craters (Riedel et al., 2020). This result also confirms the completeness of the Robbins and Hynek (2012) database for craters ≥1 km. Despite the direction for participants to pinpoint craters absent from the database during the review process, finding new craters close to the threshold diameter, i.e., 1 km, was challenging. Representing only 10 pixels in diameter on THEMIS imagery, the resolution of the data set and the precision of the manual estimation of their diameter did not allow us to add with confidence an impact crater for which the size was close to this threshold. However, the original catalog was also based on the identification of smaller craters (>500 m, >600,000 in total), which allowed the completeness of the final catalog for D (diameter) > 1 km, thus explaining the low number of new entries found by our team.

Layered Ejecta Rampart Sinuous Craters

Figure 5 shows the global distribution of SLERS, DLERS, and MLERS craters. As other researchers have previously noted (Barlow and Perez, 2003; Costard, 1989; Costard and Kargel, 1995), SLERS craters dominate the population of layered ejecta craters and are present in all Martian regions, mainly north of Alba Patera, at Lunae Planum and Tempe Terra, in Arabia Terra, and in Syrtis Major Planum.

DLERS morphologies are preferentially concentrated at midlatitudes and high latitudes, between 30° and 70°, in both hemispheres, and they are particularly concentrated on the northern plains. MLERS craters are primarily concentrated in cratered highlands, especially in the area covering the northern part of Hellas Planitia, Terra Simeria, Sinai Planum, and Terra Sirenum. The distribution of these three categories is similar to the one found by Barlow and Perez (2003). Our study confirms this distribution, with now the inclusion of 4751 additional SLERS, DLERS, or MLERS craters, particularly for small diameters (≤3 km in diameter) compared to the database of Robbins and Hynek. This inclusion is of particular interest because it offers the possibility to extend our comprehension of the processes responsible for such morphologies in smaller craters as well as their temporal and spatial evolution. More particularly, the dating of a large portion of the impact craters classified in all of these categories would allow the tracking of the presence and depth of the volatile-rich layer in the subsurface at the moment of the impact, which is suspected to have played a major role in their formation (Costard, 1989; Barlow et al., 2000), and this will complete the study performed by Jones and Osinski. (2015) in the mapping of this layer. Such investigation is currently ongoing (Benedix et al., 2020b) and made possible by the semi-automatic dating technique developed by Benedix et al. (2020a) and Lagain et al. (2021).

In a general point of view, LERS craters are widely represented around 10 km of diameter (see Figs. 3 and 6). Their size distribution decreases gradually from this size. The resolution of THEMIS data could nonetheless lead to an underestimation of the smallest LERS craters, for D < 2 km. Some craters were classified here differently from the Robbins and Hynek's database due to a different morphological interpretation; several examples of different classifications are given in Supplemental Material Appendix E. The size-frequency distribution (SFD) for DLERS craters obtained from the present survey (Fig. 6) is very close to that observed by Robbins and Hynek (2012), while that of MLERS craters follows the same trend as Robbins and Hynek's database for D > 20 km and that of Barlow et al. (2000) for D < 10 km. Our database presents a continuum linking both distributions between 10 and 20 km concerning the MLERS morphology. Our classification of the SLERS category presents the largest SFD difference compared to other databases (Fig. 6). The SFD of the SLERS category is similar to the database of Robbins and Hynek between 3 and 10 km in diameter and closer to Barlow et al.'s database for D > 10 km. Finally, SLERS craters smaller than 3 km follow the same trend as the craters with D = 3–8 km. The inclusion of 32 LARLE impact craters compared to the previous survey performed by Barlow et al. (2014) confirms the general size-frequency and geographic distribution observed in the past (Fig. 6). The SFD shows a peak around 3–4 km. The lower number of craters for a particular bin size in our database compared that of Barlow et al.'s database is due to a different diameter measurement used in both databases.

Buried/Degraded Craters

The population of buried/degraded impact craters represents 24,530 entries (6.4%) of the database. This type of impact crater

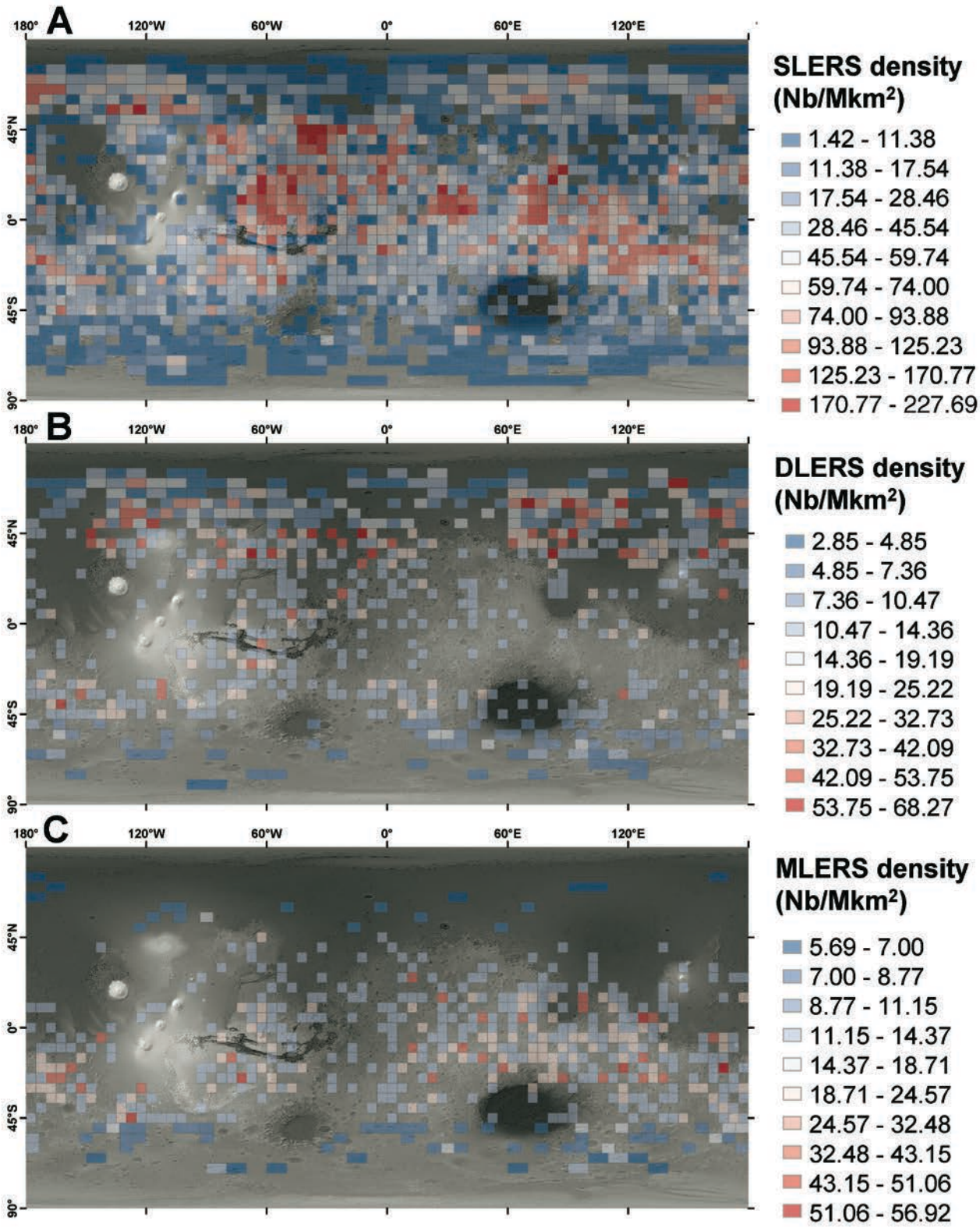

Figure 5. Distribution of the three categories of layered ejecta rampart sinuous craters in each 500,000 quadrangle. Crater density is given in number per million square kilometers. (A) Density of single layered ejecta rampart sinuous (SLERS) craters. This map shows that SLERS are highly represented on the entire surface except on the Tharsis region. (B) Double layered ejecta rampart sinuous (DLERS) crater density map shows that this type of crater is preferentially distributed at high latitudes. (C) Multiple layered ejecta rampart sinuous (MLERS) crater density map reveals that this type of crater is preferentially located on highland-plains and near the dichotomy boundary.

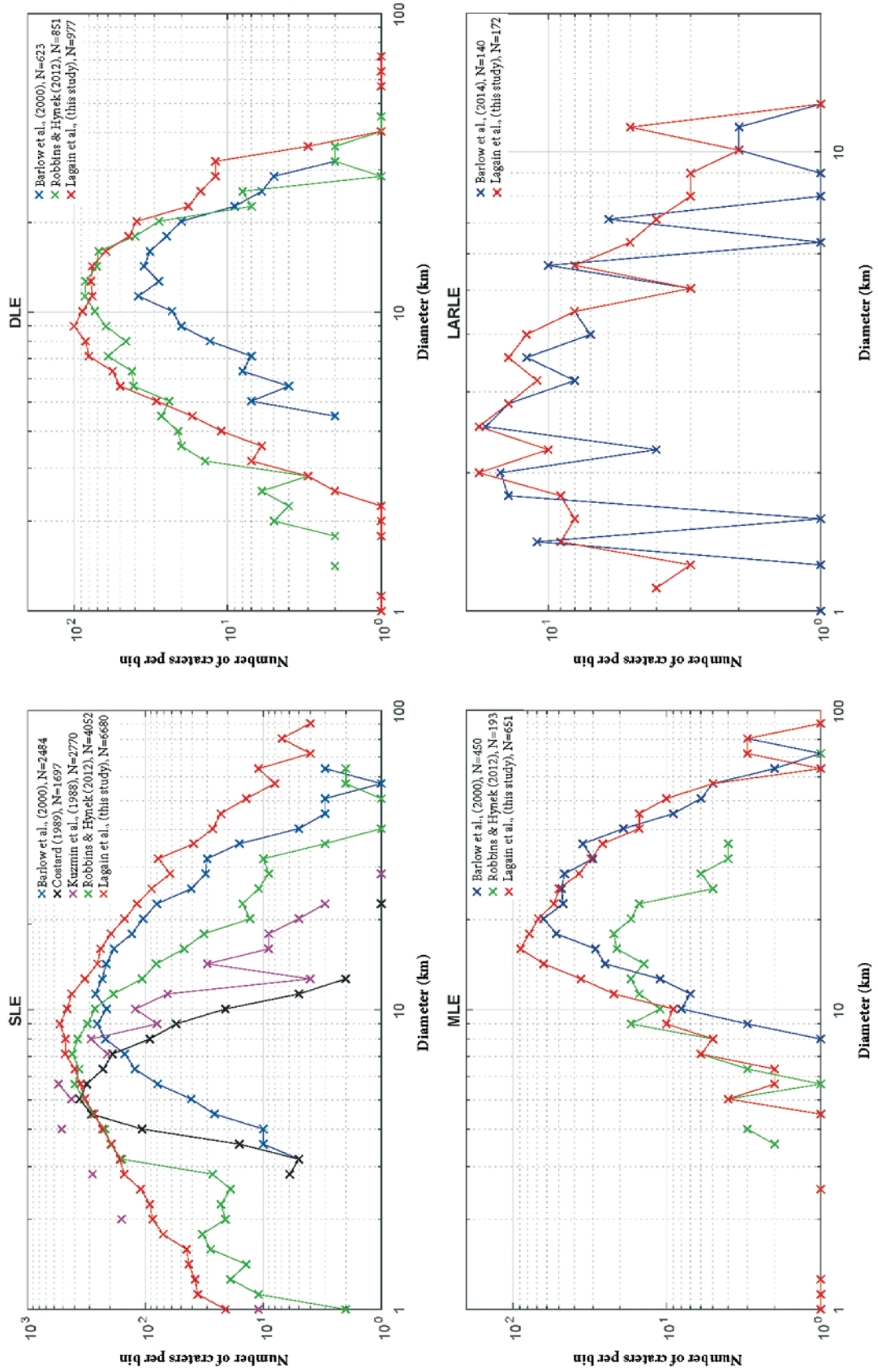

Figure 6. Size-frequency distribution of single (SLE), double (DLE), and multiple layered ejecta (MLE) rampart sinuous and low-aspect-ratio layer ejecta (LARLE) impact craters identified in this study and comparison with other databases.

is obviously primarily concentrated on highlands (Fig. 4B), where the surface is more than 3.5 b.y. old. This is consistent with the fact that these craters are also generally old. Unlike other types of craters, an increasing fraction of buried/degraded craters is observed at high latitudes. This observation is consistent with the increased efficiency of resurfacing processes in these areas. Their SFD exhibits an approximately flat distribution between 1 and 10 km (Fig. 3). For impact craters larger than 20 km, those belonging to the "buried/degraded" category are as common as those belonging to the "standard" category. Above 50 km diameter, buried craters dominate the whole population. This information could be used in future studies to examine degradation rates versus cratering rates on Mars. Even if this type of impact crater is generally removed from crater counts, they can be taken into account for dating underlying/buried geological units (Greeley and Fagents, 2001; Frey et al., 1979). The distinction between buried and not superposed impact craters in this category is impossible to make in a catalog because it depends on what part of the structure one is studying. We therefore invite users of our database to examine if they need to include or exclude these craters from the database depending on the focus of their investigation. This can be easily done from the interface we developed in this study. A possible outcome of the classification performed here is the improvement of the local erosion rate estimation on Mars through a careful analysis of the local spatial distribution of these craters and their relationships with datable surrounding terrains. This can be performed using automatic extraction of the elevation of each crater floor and rim and that of the surrounding ground using methods developed by Breton et al. (2019).

Secondary Impact Craters

Among the 384,399 entries contained in the original database, 55,309 impact craters larger than 1 km in diameter were identified as secondary craters. This is 16,700 fewer than the survey performed by Robbins and Hynek (2014). Some differences in secondary crater identification between both databases are presented in Supplemental Material Appendix A. The main differences are found for isolated craters, for which the morphologic characteristics were insufficient to classify them in this category. For secondary crater clusters, we estimated their potential link to a large primary crater by visually analyzing the direction of their asymmetric shape, thus indicating the direction of their ejection source. For the first time, 38,760 of these secondary craters (70%) were connected to 108 primary impact craters. The entire population of craters identified as secondaries in our survey is distributed on the cratered highlands and around Lyot, Lomonosov, and Mie craters north of the hemispheric dichotomy (Figs. 4C and 7A). The area in the north of Isidis Planitia concentrates a large number of secondaries associated with the Lyot crater, located northwest of this area, as already shown by Robbins and Hynek (2011a). Their size distribution shown, as on Figure 3, exhibits a steeper slope than for "standard" craters, confirming the observations of Robbins and Hynek (2014). The established association between secondary craters and their primary crater can potentially complete conclusions of Robbins and Hynek (2011b) and those of Watters et al. (2017), where the authors investigated the relationship between the secondary morphometry and the characteristics of the primary impact crater. Figure 8 presents the secondary SFD based on the impacted terrain type according to the *Geological Map of Mars* (Tanaka et al., 2014) and based on the size of the associated primary crater. If any correlation can be established between the terrain type chosen here and the size-distribution of secondary craters, the size of the primary crater is naturally linked to the production of secondaries, thus extending results from Robbins et al. (2014) to a wider crater population. Large primary craters produce large secondary craters, with an SFD flatter than that produced by a smaller impact. The lack of small secondaries produced by large craters is due to the older age of large primary craters and therefore the erosion of their associated small secondaries. Further investigations on the physical properties of the impacted material would potentially allow us to better constrain our knowledge of the factors controlling the secondary crater production, and reciprocally infer the structural properties of the ground at the moment of the impact, but also the local erosion rate evolution (Breton et al., 2018). One of the most unexpected secondary crater SFDs observed in this survey is that of Lomonosov crater, where its associated small secondary crater population (1–3 km) is underrepresented (Figs. 7B and 8B) compared to other craters of the same size and age range (~100 km, >1 Ga) located on the northern lowlands such as Mie or Milankovic. The hypothesis according to which the impact that formed this crater occurred in a shallow ocean (Costard et al., 2019) and generated the tsunami deposits observed in northwestern Arabia Terra (Rodriguez et al., 2016; Costard et al., 2017) could potentially explain the observed SFD of secondaries. Indeed, the debris ejection following the impact into a shallow aqueous layer could exhibit a limit in terms of quantity of small fragments forming secondary craters around the primary impact structure compared to an impact into a dry and strong geological layer due to water resurge (Ormö et al., 2010; Watters et al., 2017). The relationships established in the present study open new perspectives for understanding the emplacement dynamics of this type of crater and the characteristics of the impacted material.

Misidentified Entries

In the database of Robbins and Hynek, 8145 entries were flagged in our survey as not being impact craters. Some examples are given in Supplemental Material Appendix F. As shown on Figure 4D, misidentified entries are essentially concentrated on rough terrains, near the dichotomy, and on volcano-tectonic provinces where pseudocircular geological shapes are frequent. As already pointed in Robbins et al. (2014), identification of impact craters in heavily modified terrains is subject to a high variability rate in the distinction between impact craters and other geological structures. In this, the observed spatial distribution is not astonishing. The database of Robbins and Hynek includes a

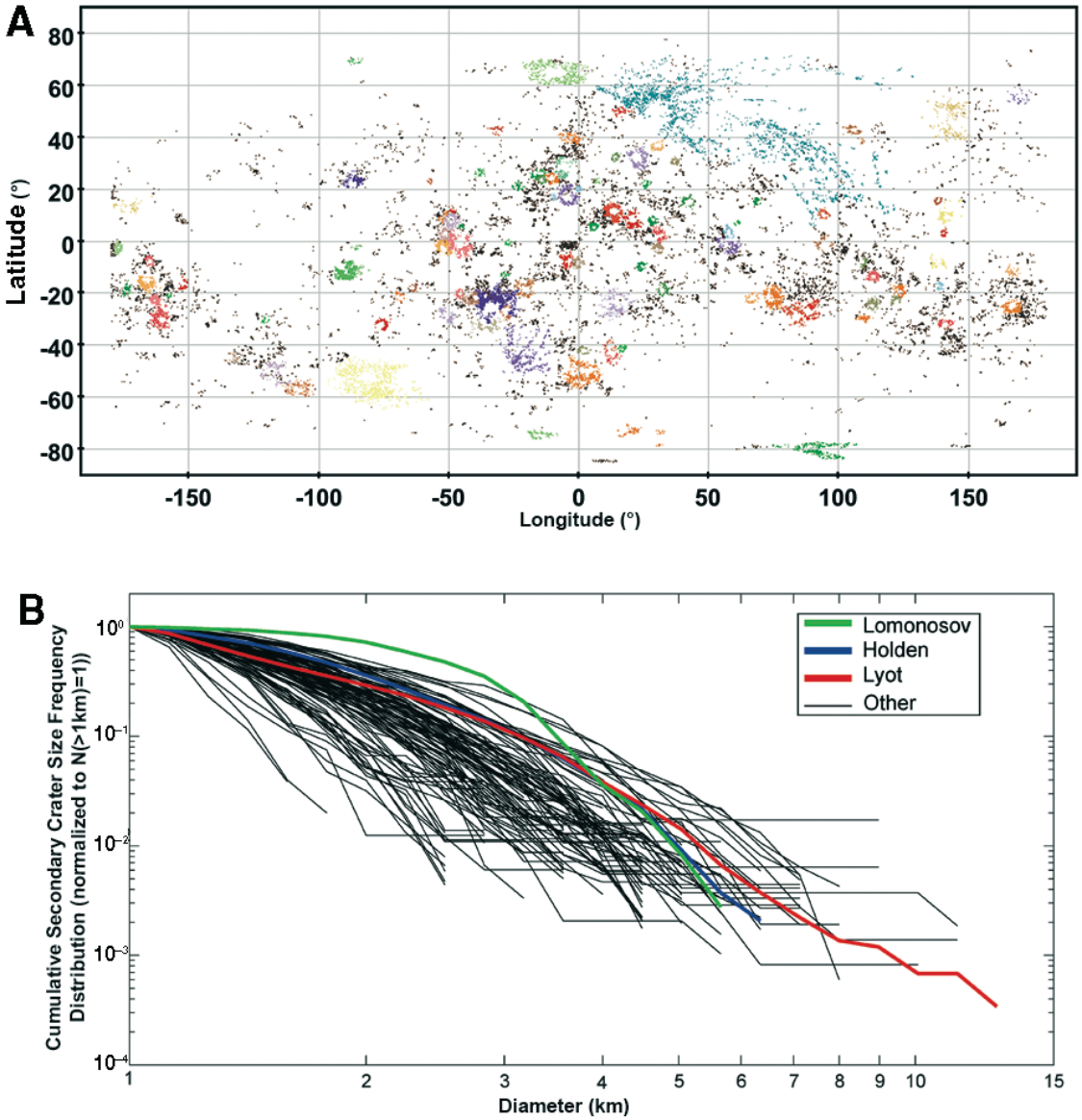

Figure 7. (A) Geographic distribution of secondary impact craters linked to their primary crater source. The color code corresponds to the secondary crater population associated with each large primary crater. (B) Cumulative secondary impact crater size-frequency distribution sorted by their primary crater origin. Small secondary crater size-frequency distribution between 1 and 3 km produced by Lomonosov crater exhibits a flatter trend compared to those from other large impact craters such as Holden and Lyot.

confidence index describing a subjective certainty that a crater is an impact crater. However, only 1294 entries have an index suggesting that they may not be impact craters. Some of them, recognized as misidentified entries in our database, do correspond to geological structures that have a shape evoking an impact crater, but that likely correspond to skylights on a tube-fed lava flow or collapsing or thermokarstic structures. Some entries do not even correspond to any visible structures at the surface, whether with THEMIS or MOLA data (some examples are shown in Supplemental Material Appendix F). These misidentified entries could have arisen from geographic coordinate errors. An error in geographic coordinates may lead in this work to the removal of one entry that is compensated by a new entry elsewhere, but this guess is impossible to verify. Nevertheless, no correspondence could be established, for instance, between added entries in our database or impact craters located at opposite coordinates (longitudes and/or latitudes, due to a sign error, for instance) and those originally mentioned in the database.

Figure 3 shows an SFD trend for this category that is quite different from the most common category of craters, i.e., standard

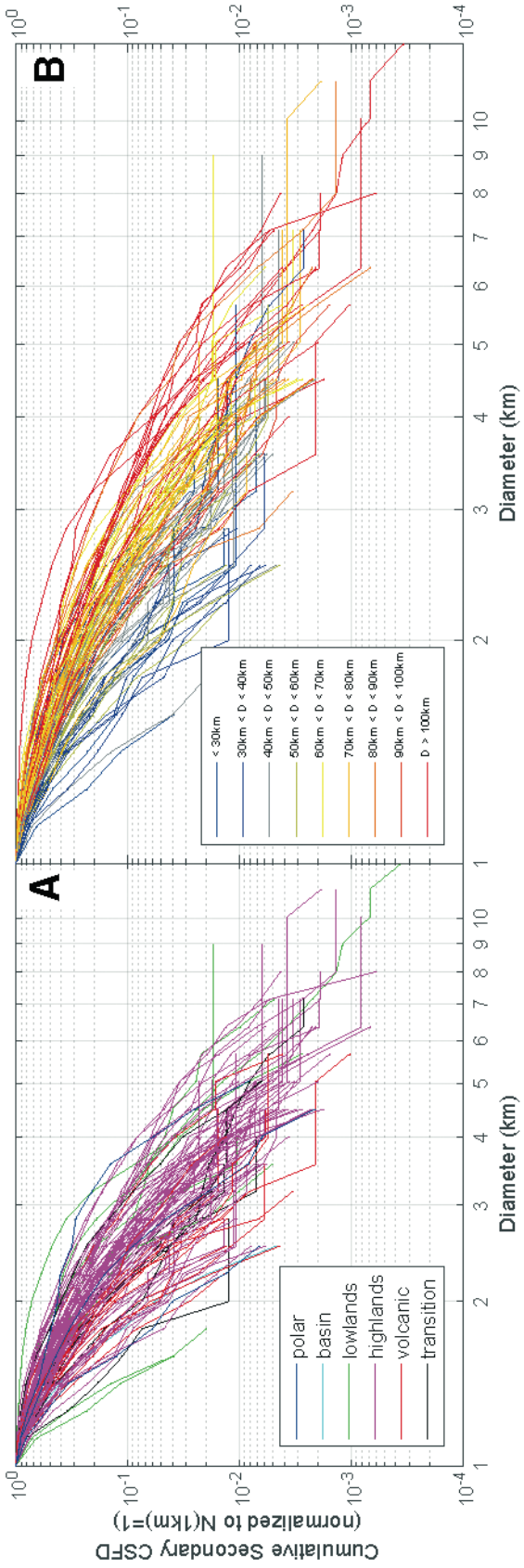

Figure 8. (A) Cumulative secondary impact crater size-frequency distribution (CSFD) sorted by primary crater origin and the impacted terrain type according to the *Geologic Map of Mars* (Tanaka et al., 2014) and (B) color coded based on the size of the associated primary impact crater.

craters. The mean slope of the distribution of misidentified entries is lower than the mean slope for other craters. This observation consolidates our interpretation about the source of misidentified entries in the original database. Entries in the original database that are not impact craters should produce an SFD that is notably different from impact craters, and this is what we observe in this study. The confusion between volcanic or tectonic features and impact craters and entries that do not correspond to any circular structure can give rise to a size distribution essentially controlled by the size of pseudocircular shapes. A blind inclusion of these entries to date some parts of the Martian surface can lead to an overestimation of its age, especially for volcanic and tectonic regions. Nevertheless, the fraction of misidentified entries is only 2% of the entire database. This very low fraction, compared to the identification variability determined by Robbins et al. (2014) (up to 30% for subkilometric craters on heavily modified terrains), can be explained in the same way as the low number of new entries (see section on "Standard Impact Craters and Added Entries"): The identification of large craters is easier than identification of smaller ones due to the underrepresentation of pseudocircular structures other than impact craters at this size scale. We expect other misidentified entries that could be spotted by the users of the database. We therefore strongly encourage the users of the database to create a pull request on the Github repository containing the crater database with their own modification of the catalog.

CONCLUSIONS, MARTIAN CRATER DATABASE AVAILABILITY, AND PERSPECTIVES

The identification of misidentified entries in the previous version of the largest Martian crater database and the morphological classification of buried/degraded and secondary craters provide to planetary geologists a complementary tool with which to quickly date geological units on the Martian surface. The identification of the primary crater source of secondary craters opens perspectives for new studies on the spatial distribution and characteristics of secondary craters and also the study of the rheology of the impacted material. Layered ejecta crater identification smaller than 3 km diameter will complete our understanding of the factors affecting the distribution of this type of ejecta and could help us to understand their formation processes. This database could also be used to improve automatic detection of crater algorithms to complete this catalog with smaller craters, with the aim to improve the temporal and spatial resolution of studies involving age derivation of Martian surfaces (Benedix et al., 2020a; Lagain et al., 2020b).

A perfect database of Martian craters will probably never exist, unless each structure could be verified in the field, as done for terrestrial impact structures (not even mentioning that some terrestrial structures are currently debatable and debated). Therefore, different views and opinions are needed to progress and warn the new users that none of the available Martian crater database can be considered to be 100% correct.

The interface developed in this study offers the possibility to the community to complete and revise our classification as well as other crater databases developed in the past, on Mars or on other planetary bodies such as the Moon, as different global higher-resolution data sets are produced, such as the recent CTX global mosaic (Dickson et al., 2018). Consequently, we strongly encourage any completion or revision of our classification by using the interface and the database we present in this study. Any improvement can be implemented to the existing database on a simple request through the Github open repository created for this project (https://github.com/alagain/martian_crater_database). Widely used computer tools for crater counting and dating planetary surfaces include CraterTools (Kneissl et al., 2011) and CraterStats II (Michael and Neukum, 2010). We therefore distributed our database by respecting the architecture of inputs readable by these software packages in order to facilitate their integration in future studies. To this purpose, secondary, degraded craters and misidentified entries are flagged as "marked," and craters classified in the "standard" category and LERS craters are flagged as "standard," in agreement with the architecture of these tools.

The catalog is also available as an interoperable data service compliant with the Virtual Observatory (VO) environment. More specifically, all parameters are described using standard metadata from the Europlanet Core (EPNCore) Data Model, and the service is responsive to the EPN-TAP access protocol (Erard et al., 2018, 2020). It can therefore be queried by several VO tools, in particular, by the VESPA portal (http://vespa.obspm.fr), which queries all such services together and can pass selections of data to VO tools with graphical capabilities, such as TOPCAT or Aladin, which in turn make it very easy to compare answers from related data services. Obvious applications include comparisons between several crater catalogs, but also more complex applications such as integration of craters of a given size range inside spatial units (with direct applications to unit dating) or, conversely, extraction of features located inside craters (e.g., gullies, flows, etc.).

Finally, a complete documentation of the interface is available at https://github.com/epn-vespa/cesium/wiki, and a demo instance is available at http://134.158.75.177/viewer/Apps/PlanetaryCesiumViewer/index.html. This offers a flexible way to work on other data sets and create a multiclassification of other planetary features usable within the research communities and adapted to citizen research projects (Jones, 2019; Keshavan et al., 2019), and it can even lead to a training data set for feature recognition using deep learning techniques (Benedix et al., 2020a).

ACKNOWLEDGMENTS

We declare no conflict of interest. We thank Joan Florsheim for the editorial handling of this manuscript, as well as C. Koerbel for helpful comments that improved this manuscript. We also appreciate the valued reviews from G. Michael, which benefited this presentation. We are also grateful to C. Fassett, N. Barlow, S. Robbins, and two anonymous reviewers for reviews of an earlier version of this manuscript. This research was funded by the GEOPS laboratory and the Domaine d'Intérêt Majeur pour l'Astrophysique et les Conditions d'Apparition de la Vie (DIM ACAV), the Australian Research Council (FT170100024), and Curtin University (Perth, Western Australia, Australia). The Europlanet-2020 and Europlanet-2024 Research Infrastructure projects have received funding from the European Union's Horizon 2020 research and innovation program under grant agreements 654208 and 871149. This work made use of the U.S. Geological Survey Web Map Service, http://planetarymaps.usgs.gov. The catalog used for analyses in this paper is available at https://doi.org/10.5281/zenodo.3633594. The EPN-TAP data service is installed and maintained at Jacobs University, Bremen, Germany. The interface used for the crater classification, for which the link is mentioned in the main text, is usable on the latest version of Google Chrome or Mozilla Firefox.

REFERENCES CITED

Barata, T., Alves, E.I., Machado, A., and Barberes, G.A., 2012, Characterization of palimpsest craters on Mars: Planetary and Space Science, v. 72, p. 62–69, https://doi.org/10.1016/j.pss.2012.09.015.

Barlow, N.G., 1995, The degradation of impact craters in Maja Valles in Arabia, Mars: Journal of Geophysical Research, v. 100, p. 23,307–23,316, https://doi.org/10.1029/95JE02492.

Barlow, N.G., 2004, Martian subsurface volatile concentrations as a function of time: Clues from layered ejecta craters: Geophysical Research Letters, v. 31, L05703, https://doi.org/10.1029/2003GL019075.

Barlow, N.G., 2017, Revision of the "Catalog of large Martian impact craters" and comparison to other Martian crater databases, *in* Proceedings of the 48th Lunar and Planetary Science Conference: Houston, Texas, Lunar and Planetary Institute, abstract 1562.

Barlow, N.G., and Bradley, L., 1990, Martian impact craters: Correlation of ejecta and interior morphologies with diameter, latitude and terrain: Icarus, v. 87, p. 156–179, https://doi.org/10.1016/0019-1035(90)90026-6.

Barlow, N.G., and Perez, C.B., 2003, Martian impact crater ejecta morphologies as indicators of the distribution of subsurface volatiles: Journal of Geophysical Research–Planets, v. 108, no. E8, 5085, https://doi.org/10.1029/2002JE002036.

Barlow, N.G., Boyce, J.M., Costard, F.M., Craddock, R.A., Garvin, J.B., Sakimoto, S.E.H., Kuzmin, R.O., Roddy, D.J., and Soderblom, L.A., 2000, Standardizing the nomenclature of Martian impact crater ejecta morphologies: Journal of Geophysical Research–Planets, v. 105, no. E11, p. 26733–26738, https://doi.org/10.1029/2000JE001258.

Barlow, N.G., Boyce, J.M., and Cornwall, C., 2014, Martian low-aspect-ratio layered ejecta (LARLE) craters: Distribution, characteristics, and relationship to pedestal craters: Icarus, v. 239, p. 186–200, https://doi.org/10.1016/j.icarus.2014.05.037.

Benedix, G.K., Lagain, A., Chai, K., Meka, S., Anderson, S., Norman, C., Bland, P.A., Paxman, J., Towner, M.C., and Tan, T., 2020a, Deriving surface ages on Mars using automated crater counting: Earth and Space Science, v. 7, e2019EA001005, https://doi.org/10.1029/2019EA001005.

Benedix, G.K., Lagain, A., Chai, K., Meka, S., Norman, C., Anderson, S., Bland, P.A., Paxman, J., Towner, M.C., Servis, K., and Sansom, E.K., 2020b, Martian impact crater database: Towards a complete dataset of $D > 100$ m and automatic identification of secondary craters clusters, *in* Proceedings of the 51st Lunar and Planetary Science Conference: Houston, Texas, Lunar and Planetary Institute, abstract 2007.

Boyce, J.M., Wilson, L., and Barlow, N.G., 2015, Origin of the outer layer of Martian low-aspect ratio layered ejecta craters: Icarus, v. 245, p. 263–272, https://doi.org/10.1016/j.icarus.2014.07.032.

Breton, S., Quantin-Nataf, C., Pan, L., Bodin, T., and Bras, E., 2018, Crater depth statistics: Constraining obliteration rates from secondary clusters of Mojave crater: European Planetary Science Congress Abstracts, v. 12, abstract EPSC2018-955.

Christensen, P.R., Jakosky, B.M., Kieffer, H.H., Malin, M.C., McSween, H.Y., Jr., Nealson, K., Mehall, G.L., Silverman, S.H., Ferry, S., Caplinger, M., and Ravine, M., 2004, The Thermal Emission Imaging System (THEMIS) for the Mars 2001 Odyssey Mission: Space Science Reviews, v. 110, p. 85–130, https://doi.org/10.1023/B:SPAC.0000021008.16305.94.

Costard, F., 1989, The spatial distribution of volatiles in the Martian hydrolithosphere: Earth, Moon, and Planets, v. 45, p. 265–290, https://doi.org/10.1007/BF00057747.

Costard, F., and Kargel, J.S., 1995, Outwash plains and thermokarst on Mars: Icarus, v. 114, p. 93–112, https://doi.org/10.1006/icar.1995.1046.

Costard, F., Séjourné, A., Kelfoun, K., Clifford, S., Lavigne, F., Di Pietro, I., and Bouley, S., 2017, Modeling tsunami propagation and the emplacement of thumbprint terrain in an early Mars ocean: Journal of Geophysical Research–Planets, v. 122, no. 3, p. 633–649, https://doi.org/10.1002/2016JE005230.

Costard, F., Séjourné, A., Lagain, A., Ormö, J., Rodriguez, J.A.P., Clifford, S., Bouley, S., Kelfoun, K., and Lavigne, F., 2019, The Lomonosov Crater impact event: A possible mega-tsunami source on Mars: Journal of Geophysical Research–Planets, v. 124, no. 9, p. 1840–1851, https://doi.org/10.1029/2019JE006008.

Craddock, R., Maxwell, T., and Howard, A.D., 1997, Crater morphometry and modification in the Sinus Sabaeus and Margaritifer Sinus regions of Mars: Journal of Geophysical Research, v. 102, p. 13,321–13,340, https://doi.org/10.1029/97JE01084.

Crater Analysis Techniques Working Group, 1979, Standard techniques for presentation and analysis of crater size-frequency data: Icarus, v. 37, p. 467–474, https://doi.org/10.1016/0019-1035(79)90009-5.

Dickson, J.L., Kerber, L.A., Fassett, C.I., and Ehlmann, B.L., 2018, A global, blended CTX mosaic of Mars with vectorized seam mapping: A new mosaicking pipeline using principles of non-destructive image editing, *in* Proceedings of the 49th Lunar and Planetary Science Conference: Houston, Texas, Lunar and Planetary Institute, abstract 2480.

Erard, S., Cecconi, B., Le Sidaner, P., Rossi, A.P., Capria, M.T., Schmitt, B., Génot, V., André, N., Vandaele, A.C., Scherf, M., Hueso, R., Määttänen, A., Thuillot, W., Carry, B., Achilleos, N., Marmo, C., Santolik, O., Benson, K., Fernique, P., Beigbeder, L. Millour, E., Rousseau, B., Andrieu, F., Chauvin, C., Minin, M., Ivanoski, S., Longobardo, A., Bollard, P., Albert, D., Gangloff, M., Jourdane, N., Bouchemit, M., Glorian, J.-M., Trompet, L., Al-Ubaidi, T., Juaristi, J., Desmars, J., Guio, P., Delaa, O., Lagain, A., Soucek, J., and Pisa, D., 2018, VESPA: A community-driven Virtual Observatory in planetary science: Planetary and Space Science, v. 150, p. 65–85, https://doi.org/10.1016/j.pss.2017.05.013.

Erard, S., Cecconi, B., Le Sidaner, P., Chauvin, C., Rossi, A.P., Minin, M., Capria, T., Ivanovski, S., Schmitt, B., Génot, V., André, N., Marmo, C., Vandaele, A.C., Trompet, L., Scherf, M., Hueso, R., Määttänen, A., Carry, B., Achilleos, N., Soucek, J., Pisa, D., Benson, K., Fernique, P., and Millour, E., 2020, Virtual European Solar & Planetary Access (VESPA): A planetary science virtual observatory cornerstone: Data Science Journal, v. 19, no. 1, p. 22, https://doi.org/10.5334/dsj-2020-022.

Farley, K.A., Malespin, C., Mahaffy, P., Grotzinger, J.P., Vasconcelos, P.M., Milliken, R.E., Malin, M., Edgett, K.S., Pavlov, A.A., Hurowitz, J.A., Grant, J.A., et al., 2014, In situ radiometric and exposure age dating of the Martian surface: Science, v. 343, 1247166, https://doi.org/10.1126/science.1247166.

Frey, H., Lowry B.L., and Chase, S.A., 1979, Pseudocraters on Mars: Journal of Geophysical Research, v. 84, p. 8075–8086, https://doi.org/10.1029/JB084iB14p08075.

Greeley, R., and Fagents, S., 2001, Icelandic pseudocraters as analogs to some volcanic cones on Mars: Journal of Geophysical Research, v. 106, p. 20,527–20,546, https://doi.org/10.1029/2000JE001378.

Hartmann, W., and Neukum, G., 2001, Cratering chronology and the evolution of Mars: Space Science Reviews, v. 96, p. 165–194, https://doi.org/10.1023/A:1011945222010.

Jones, E., 2019, A battle between machine learning, traditional clustering and citizen scientists in the detection and segmentation of polar spring-time fans on Mars, *in* Proceedings of the 19th Australian Space Research Conference, Adelaide, South Australia, Australia.

Jones, E., and Osinski, G., 2015, Using Martian single and double layered ejecta craters to probe subsurface stratigraphy: Icarus, v. 247, p. 260–278, https://doi.org/10.1016/j.icarus.2014.10.016.

Kadish, S.J., and Head, J.W., 2014, The ages of pedestal craters on Mars: Evidence for a late-Amazonian extended period of episodic emplacement of decameters-thick mid-latitude ice deposits: Planetary and Space Science, v. 91, p. 91–100, https://doi.org/10.1016/j.pss.2013.12.003.

Keshavan, A., Yeatman, J.D., and Rokem, A., 2019, Combining citizen science and deep learning to amplify expertise in neuroimaging: Frontiers in Neuroinformatics, v. 13, p. 29, https://doi.org/10.3389/fninf.2019.00029.

Kneissl, T., Gasselt, S. van, and Neukum, G., 2011, Map-projection-independent crater size-frequency determination in GIS environments: New software tool for ArcGIS: Planetary and Space Science, v. 59, p. 1243–1254, https://doi.org/10.1016/j.pss.2010.03.015.

Kuzmin, R.O., Bobina, N.N., Zabalueva, E.V., and Shashkina, V.P., 1988, Structural inhomogeneities of the Martian cryosphere: Solar System Research, v. 22, p. 121–133.

Lagain, A., Bouley, S., Baratoux, D., Costard, F., and Wieczorek, M., 2020a, Impact cratering rate consistency test from ages of layered ejecta on Mars: Planetary and Space Science, v. 180, 104755, https://doi.org/10.1016/j.pss.2019.104755.

Lagain, A., et al., 2020b, Automatic crater detection over the Jezero crater area from HiRISE imagery, *in* Proceedings of the 51st Lunar and Planetary Science Conference: Houston, Texas, Lunar and Planetary Institute, abstract 2069.

Lagain, A., Servis, K., Benedix, G.K., Norman, C., Anderson, S., and Bland, P.A., 2021, Model age derivation of large Martian impact craters, using automatic crater counting methods: Earth and Space Science, v. 8, e2020EA001598, https://doi.org/10.1029/2020EA001598.

Lee, C., 2019, Automated crater detection on Mars using deep learning: Planetary and Space Science, v. 170, p. 16–28, https://doi.org/10.1016/j.pss.2019.03.008.

McEwen, A., and Bierhaus, E., 2006, The importance of secondary cratering to age constraints on planetary surfaces: Annual Review of Earth and Planetary Sciences, v. 34, p. 535–567, https://doi.org/10.1146/annurev.earth.34.031405.125018.

Michael, G.G., and Neukum, G., 2010, Planetary surface dating from crater size frequency distribution measurements: Partial resurfacing events and statistical age uncertainty: Earth and Planetary Science Letters, v. 294, p. 223–229, https://doi.org/10.1016/j.epsl.2009.12.041.

Oberbeck, V.R., and Morrison, R.H., 1974, Laboratory simulation of the herring-bone pattern associated with lunar secondary crater chains: The Moon, v. 9, p. 415–455, https://doi.org/10.1007/BF00562581.

Ormö, J., Lepinette, A., Sturkell, E., Lindström, M., Housen, K.R., and Holsapple, K.A., 2010, Water resurge at marine-target impact craters analyzed with a combination of low-velocity impact experiments and numerical simulations, *in* Gibson, R.L., and Reimold, W.U., eds., Large Meteorite Impacts and Planetary Evolution IV: Geological Society of America Special Paper 465, p. 81–101, https://doi.org/10.1130/2010.2465(06).

Pietrek, A., Wulf, G., and Kenkmann, T., Detailed geological mapping (1:80,000-scale) of Steinheim crater, Mars, *in* Proceedings of the 44th Lunar and Planetary Science Conference: Houston, Texas, Lunar and Planetary Institute, abstract 1465.

Quantin, C., Popova, O., Hartmann, W.K., and Werner, S.C., 2016, Young Martian crater Gratteri and its secondary craters: Journal of Geophysical Research–Planets, v. 121, no. 7, p. 1118–1140, https://doi.org/10.1002/2015JE004864.

Riedel, C., Minton, D.A., Michael, G., Orgel, C., van der Bogert, C.H., and Hiesinger, H., 2020, Degradation of small simple and large complex lunar craters: Not a simple scale dependence: Journal of Geophysical Research, v. 125, no. 4, e2019JE006273, https://doi.org/10.1029/2019JE006273.

Robbins, S.J., and Hynek, B.M., 2011a, Distant secondary craters from Lyot crater, Mars, and implications for surface ages of planetary bodies: Geophysical Research Letters, v. 38, L05201, https://doi.org/10.1029/2010GL046450.

Robbins, S.J., and Hynek, B.M., 2011b, Secondary crater fields from 24 large primary craters on Mars: Insights into nearby secondary crater production: Journal of Geophysical Research, v. 116, E10003, https://doi.org/10.1029/2011JE003820.

Robbins, S.J., and Hynek, B.M., 2012, A new global database of Mars impact craters ≥1 km: 1. Data creation, properties, and parameters: Journal of Geophysical Research, v. 117, E05004, https://doi.org/0.1029/2011JE003966.

Robbins, S.J., and Hynek, B.M., 2014, The secondary crater population of Mars: Earth and Planetary Science Letters, v. 400, p. 66–76, https://doi.org/10.1016/j.epsl.2014.05.005.

Robbins, S.J., Antonenko, I., Kirchoff, M.R., Chapman, C.R., Fassett, C.I., Herrick, R.R., Singer, K., Zanetti, M., Lehan, C., Huang, D., and Gay, P.L.,

2014, The variability of crater identification among expert and community crater analysts: Icarus, v. 234, p. 109–131, https://doi.org/10.1016/j.icarus.2014.02.022.

Rodriguez, J.A.P., Fairen, A.G., Linares, R., Zarrroca, M., Platz, T., Komatsu, G., Kargel, J.S., Gulick, V., Jianguo, Y., Higuchi, K., Miyamoto, H., Baker, V.R., and Glines, N., 2016, Tsunami waves extensively resurfaced the shorelines of an early Martian ocean: Scientific Reports, v. 6, 25106, https://doi.org/10.1038/srep25106.

Salamunićcar, G., Lončarić, S., and Mazarico, E., 2012, LU60645GT and MA132843GT catalogues of Lunar and Martian impact craters developed using a Crater Shape–based interpolation crater detection algorithm for topography data: Planetary and Space Science, v. 60, p. 236–247, https://doi.org/10.1016/j.pss.2011.09.003.

Shoemaker, E.M., 1962, Interpretation of lunar craters, *in* Kopal, Z., ed., Physics and Astronomy of the Moon: New York, Academic Press, p. 283–359.

Shoemaker, E.M., 1965, Preliminary analysis of the fine structure of the lunar surface in Mare Cognitum, *in* Heiss, W.N., Menzel, D.R., and O'Keefe, J.A., eds., The Nature of the Lunar Surface: Baltimore, Maryland, Johns Hopkins University Press, p. 23–77.

Smith, D.E., and 23 others, 2001, Mars Orbiter Laser Altimeter: Experiment summary after the first year of global mapping of Mars, Journal of Geophysical Research, v. 106, no. E10, p. 23,689–23,722, https://doi.org/10.1029/2000JE001364.

Tanaka, K.L., Skinner, J.A., Jr., Dohm, J.M., Irwin, R.P., III, Kolb, E.J., Fortezzo, C.M., Platz, T., Michael, G.G., and Hare, T.M., 2014, Geologic Map of Mars: U.S. Geological Survey Scientific Investigations Map 3292, scale 1:20,000,000, pamphlet 43 p., https://doi.org/10.3133/sim3292.

Urbach, E.R., and Stepinski, T.F., 2009, Automatic detection of sub-km craters in high resolution planetary images: Planetary and Space Science, v. 57, p. 880–887, https://doi.org/10.1016/j.pss.2009.03.009.

Warren, A.O., Kite, E.S., Williams, J.-P., and Horgan, B., 2019, Through the thick and thin: New constraints on Mars paleopressure history 3.8–4 Ga from small exhumed craters: Journal of Geophysical Research–Planets, v. 124, no. 11, p. 2793–2818, https://doi.org/10.1029/2019JE006178.

Watters, W.A., Hundal, C.B., Radford, A., Collins, G.S., and Tornabene, L., 2017, Dependence of secondary crater characteristics on downrange distance: High-resolution morphometry and simulations: Journal of Geophysical Research–Planets, v. 122, no. 8, p. 1773–1800, https://doi.org/10.1002/2017JE005295.

Manuscript Accepted by the Society 6 November 2020
Manuscript Published Online 19 March 2021

Printed in the USA